Proactive Stability Augmentation for Voluntary Human Motion: Validations on a Hip Exoskeleton in Leaning and Slip Perturbations

***Abstract*—Ensuring gait stability is crucial for safe and effective human locomotion. However, the vast majority of control paradigms for lower-limb exoskeletons are developed and validated under steady, nominal walking, and their performance under unstable gait conditions or external perturbations remains unclear. In addition, many existing gait stability augmentation approaches are task-specific or rely on pre-defined reference kinematics, which can limit their generalizability and constrain the user's voluntary motion. In this paper, we present a control framework for gait stability augmentation in lower-limb exoskeletons that improves locomotion stability while preserving voluntary motion. The proposed framework defines a center of mass-based stability indicator, and employs control barrier functions to enforce safety constraints on its state, which is characterized by CoM position and velocity, without prescribing reference kinematics. Assistance is generated when the system state approaches the boundary of the safety set, thereby enabling proactive intervention to preserve stability. To account for voluntary human motion, we propose a nonlinear disturbance observer to estimate human joint torques, and their estimates are incorporated into the control design. Experiments were conducted with four non-disabled subjects wearing a bilateral hip exoskeleton performing leaning tasks as well as treadmill walking with randomly timed slip perturbations. Ensemble-averaged muscle efforts showed average reductions of 41% (leaning) and 21% (slipping), along with reductions in peak-to-peak whole-body angular momentum and shorter recovery time, indicating the effectiveness of the proposed approach in augmenting gait stability across locomotion tasks and perturbation conditions.**

***Index Terms*—Prosthetics & exoskeletons, wearable robotics, optimization & optimal control, human performance augmentation.**

I. Introduction

FALLS and falls-related injuries constitute a major public health concern across all age groups. Globally, falls account for more than 600,000 deaths each year [1]. Beyond mortality, falls frequently lead to severe health consequences, for instance, unintentional falls account for nearly half of nonfatal traumatic brain injury-related hospitalizations [2]. In particular, slip-related events comprise 40% of outdoor falls in elderly individuals and can result in serious injuries such as hip fracture [3]. These statistics highlight the importance of developing assistive technologies capable of improving gait stability and reducing fall risk during locomotion.

Conventional assistive devices, such as canes and walkers, ankle-foot orthoses, and hip protectors, primarily provide passive assistance to increase the base of support, constrain joint motion, or mitigate injury after a fall [4], [5]. However, these devices are generally not designed to actively assist users in destabilizing events, which are a major contributor to fall-related injuries. Their effectiveness and adaptability remain limited in practice. For instance, canes and walkers require continuous grasping, which restricts the users' upper-limb motion and thus hinders their mobility. While passive ankle-foot orthoses can improve certain gait stability metrics in clinical populations, they cannot provide active assistance to restore missing functions of impaired limbs [6]. Devices such as hip protectors can reduce the risk of hip fracture, but do not directly contribute to preventing falls [5]. These limitations motivate the development of active assistive technologies capable of supporting users during destabilizing locomotion.

Emerging powered lower-limb exoskeletons have demonstrated strong potential in assisting human users during both steady-state [7] and perturbed conditions [8]. A variety of assistive strategies have been proposed to enhance locomotion safety and stability, yet limitations persist. Reactive strategies provide assistance in response to detected perturbations. For example, the "help-when-needed" control paradigm enables an exoskeleton to assist balance recovery with minimal subject-specific customization once a perturbation such as a slip is detected [8]. However, the pre-defined assistive torques used in such approaches typically do not account for users' voluntary responses during destabilizing events. In contrast, bio-inspired approaches attempt to replicate human neuromuscular responses to perturbations. For instance, Afschrift et al. proposed an ankle exoskeleton controller that estimates and compensates for muscle-like ankle torques to assist balance recovery during perturbed walking [9]. While such approaches can reproduce aspects of human reactive behaviors, human responses to perturbations are not always optimal, since psychological factors such as fear of falling may lead to transient reactions that increase fall risk [10]. Moreover, since reactive assistance occurs only after instability develops, proactive strategies that anticipate or constrain unstable motion may provide more effective fall protection [11]. Learning-based techniques have also been explored. For instance, Luo et al. trained a neural network policy using deep reinforcement learning to assist walking while providing balance support [12]. However, such approaches require extensive and unbiased training data covering diverse perturbation scenarios, which are difficult to obtain for perturbed walking where unstable gait patterns are highly variable. Designing exoskeleton controllers that provide proactive stability assistance while encouraging voluntary motion under diverse perturbations remains a key challenge.

As a complementary direction that does not rely on exhaustive datasets, model-based control methods can deliver timely assistance during the brief intervals in which perturbations occur. Capture point theory has been employed to design balance control strategies under large perturbations [13]. For instance, it has been applied to correct unsafe leaning movements and avoid falls [14]. Zhu et al. further developed a control strategy based on slip recoverability regions to help

users regain balance after unexpected foot slips [15]. Despite their effectiveness in the targeted scenarios, these approaches often rely on pre-defined reference trajectories or equilibrium joint angles, which may not generalize across scenarios and can overly constrain a user's voluntary motion.

Alternative approaches have attempted to characterize balance using dynamic metrics. For example, Vallinas et al. proposed a momentum-based controller that generates assistance by minimizing changes in whole-body momentum subject to model and dynamic constraints via a quadratic program (QP) [16]. Without explicitly enforcing reference kinematics, the approach is promising in encouraging voluntary human motion, yet the standing-specific constraints limit its application on other tasks. Similarly, the extrapolated center of mass (XCoM) has been widely used for control design to provide balance assistance by enforcing an individual's CoM within the support polygon [17]. However, most XCoM relies on the linear inverted pendulum approximation with fixed eigenfrequency and approximately constant CoM height, assumptions that may be violated under larger perturbations. More recently, as a tool for safety-critical control, CBFs have gained increasing attention as a computationally efficient framework for enforcing safety constraints in real-time control systems [18], with applications ranging from dynamic balancing on a Segway-type robot [19] to achieving real-time stable walking for bipedal robots [20]. In particular, CBF has also been applied to improve gait safety by limiting the user's motion within a pre-defined range [21]. However, since the range was determined by pre-defined trajectories, translating the control strategy to different individuals and tasks becomes challenging. Overall, a key challenge is to design exoskeleton stability augmentation strategies that can assist humans across diverse perturbations without prescribing reference kinematics, while preserving the user's voluntary motion.

In this paper, we propose a stability augmentation controller (SAC) for lower-limb exoskeletons to augment gait stability without prescribing reference kinematics or overly constraining the user's voluntary motion. The approach defines a CoM-based stability indicator, which characterizes stable locomotion as the CoM and its velocity remaining within a prescribed safe region relative to the stance and swing foot locations. Stability augmentation is formulated as a safety-critical control problem, where the CoM state is constrained within this safe region using CBFs. Because the CoM represents the weighted sum of all body segments, regulating it allows users to maintain stability through self-selected gaits while preserving voluntary motion. Furthermore, the SAC acts as a torque filter that minimally modifies the nominal human torque to satisfy stability constraints, a CBF-based stability augmentation controller can minimally interfere with the user's voluntary motion during steady-state locomotion while providing rapid assistance when instability is detected. We further introduce relaxation terms in the stability indicator to preserve natural user responses under mild instability. By incorporating both position and velocity of the stability indicator into the CBF formulation, the proposed SAC can also provide assistance before unstable postures fully develop when stability is deteriorating rapidly to enable more proactive assistance, which is beneficial in assisting users during balance recovery [11]. To explicitly account for human input, we propose a novel nonlinear disturbance observer (NDO) for online estimation of human joint torques and incorporate them into control design. We implemented the proposed control strategy and conducted experiments on four non-disabled subjects wearing a powered hip exoskeleton during quasi-static leaning tasks and walking tasks with randomly timed slip perturbations. Treadmill-induced slip perturbations provided precise and repeatable control of perturbation timing and intensity, while still allowing voluntary user responses to the perturbation. Experimental results show average reductions of 41% (leaning) and 21% (slipping) in ensemble-averaged muscle efforts, along with a 9% decrease in peak-to-peak WBAM and shorter recovery time during slip perturbations. Together, these results highlight the SAC's efficacy in providing partial assistance to restore balance for individual users. The main contributions of the paper are summarized as:

- We introduce a CBF-driven SAC that directly enforces a CoM position-velocity safety set to provide proactive, minimal-intervention assistance under unstable locomotion without prescribing reference kinematics, thereby preserving voluntary human motion.
- We develop a NDO that estimates perturbation-varying human joint torques in real time and integrates these estimates into the SAC design, explicitly embedding human intent into safety-critical control.
- We implement the proposed SAC on a bilateral hip exoskeleton and validate it through human-subject experiments in leaning and randomly timed treadmill-induced slip perturbations, demonstrating reduced muscular effort, reduced WBAM deviations, and faster recovery.

The rest of the paper is organized as follows: In Sec. II, we introduce dynamics of the human-exoskeleton system, and briefly review the concept of control barrier functions. We then derive the control framework using a CoM-based control barrier function and human joint input estimation using the nonlinear disturbance observer in Sec. III. The exoskeleton system used for experimental validations is presented in Sec. IV, followed by the experimental model, protocol, and data collection procedure in Sec. V. We demonstrate experimental results in Sec. VI. Finally, conclusions are drawn in Sec. VII.

II. Preliminaries

A. Dynamics of the Human-Exoskeleton System

We model a human walking with an exoskeleton as one biped with its dynamics can be expressed as [22]

$$M\ddot{q} + C\dot{q} + N + A^{\top}\lambda = \tau + J^{\top}F_{\text{perturb}}, \tag{1}$$

where $q \in \mathbb{R}^{\mathrm{n}}$ represents the configuration vector with n being the degrees of freedom (DoFs), $M \in \mathbb{R}^{\mathrm{n}\times\mathrm{n}}$ denotes the inertia matrix, $C \in \mathbb{R}^{\mathrm{n}\times\mathrm{n}}$ is the Coriolis/centrifugal matrix, and $N \in \mathbb{R}^{\mathrm{n}}$ represents the gravitational force vector. The constraint matrix A, which is the gradient of holonomic constraint functions, maps the ground reaction forces $\lambda = \hat{\lambda} + \check{\lambda}\tau$ into the overall dynamics, where $\hat{\lambda} = W(\dot{A}\dot{q} - AM^{-1}N)$, $W = (AM^{-1}A^{\top})^{-1}$, and $\check{\lambda} = WAM^{-1}$ [22]. In (1),

all inertial parameters are the combined values of human and exoskeleton. The overall internal torque τ combines the human torque vector τ_{hum} and the exoskeleton torque vector $\tau_{\text{exo}} = Bu$, where $B = (0_{\text{p}\times(\text{n}-\text{p})},\ I_{\text{p}\times\text{p}})^\top \in \mathbb{R}^{\text{n}\times\text{p}}$ maps the exoskeleton torque $u \in \mathbb{R}^{\text{p}}$ into the system. To explicitly account for potential external perturbations, we include a wrench term $F_{\text{perturb}} \in \mathbb{R}^6$ and map it into the dynamics via a Jacobian matrix $J \in \mathbb{R}^{6\times\text{n}}$.

B. Review of Control Barrier Functions

The general form of a nonlinear system can be written as

$$\dot{x} = f(x) + g(x)u, \tag{2}$$

where $x \in \mathcal{D} \subset \mathbb{R}^{\text{n}}$ represents the state vector, $f(\cdot)$ and $g(\cdot)$ are locally Lipschitz functions with the control input $u \in \mathcal{U} \subset \mathbb{R}^{\text{m}}$ [23]. Choosing $x = [q^\top, \dot{q}^\top]^\top \in \mathbb{R}^{2\text{n}}$, (1) can be formulated in the form of (2) as

$$\dot{x} = f(x) + g(x)u = \begin{bmatrix} \dot{q} \\ M^{-1}Q \end{bmatrix} + \begin{bmatrix} 0 \\ M^{-1}B \end{bmatrix} u, \tag{3}$$

where $Q = -C\dot{q} - N - A^\top\lambda + \tau_{\text{hum}} + J^\top F_{\text{perturb}}$.

A safe set $\mathcal{C} = \{x \in \mathcal{D} \subset \mathbb{R}^{\text{n}} : h(x) \geq 0\}$ is a closed set that consists of all admissible safe states defined by a continuously differentiable barrier function $h(x) : \mathcal{D} \to \mathbb{R}$. With this definition, the system can be considered safe if the set $\mathcal{C}$ is asymptotically stable and forward-invariant in $\mathcal{D}$. Assume h (with x omitted hereafter) has relative degree one, then it is a CBF if there exists an extended class $\mathcal{K}_\infty$ function α such that for (2) and for all $x \in \mathcal{D}$,

$$\sup_{u\in U}[L_f h + L_g h u] \geq -\alpha(h), \tag{4}$$

where $L_f h$ and $L_g h$ denote Lie derivatives [23]. Any Lipschitz continuous controller u chosen from the set

$$K_{\text{cbf}}(x) = \{u \in \mathcal{U} : L_f h + L_g h u + \alpha(h) \geq 0\} \tag{5}$$

ensures the set $\mathcal{C}$ forward-invariant and asymptotically stable in $\mathcal{D}$, thereby guaranteeing safety [23].

III. Control Design

In this section, we design a CBF-based SAC to augment human walking stability under unstable postures or perturbations. Different from conventional reference kinematics based methods, this control paradigm aims to provide assistance based on the relative position of an individual's CoM to foot positions without prescribing to reference trajectories while accounting for the user's voluntary motion.

A. CoM-Based Control Barrier Function

To design a CBF for stability augmentation, we need a metric to continuously quantify gait stability. The XCoM is widely used for gait analysis and stability-oriented control design [17]. For example, the margin of stability (MoS) [24] measures gait stability as the signed distance between the XCoM and the boundary of an individual's base of support (BoS), where positive values indicate stable walking. However, conventional XCoM is derived from a simplified inverted pendulum model and typically assumes an approximately constant CoM height, which can be violated under large perturbations. Motivated by the BoS-margin interpretation of MoS, we instead define a CoM-based CBF that incorporates tolerance for natural gait variability and user-specific stabilization strategies. First, we define a stability indicator

$$\begin{aligned} s &= [\text{CoM}_x - (x_- - \delta_1)][(x_+ + \delta_2) - \text{CoM}_x], \\ x_- &= \min(p_{\text{stance},x}, p_{\text{swing},x}), \\ x_+ &= \max(p_{\text{stance},x}, p_{\text{swing},x}), \end{aligned} \tag{6}$$

where CoM_x denotes the horizontal position of CoM, and x_- and x_+ denote the horizontal positions of posterior and anterior foot boundaries, respectively. The quantities $p_{\text{stance},x}$ and $p_{\text{swing},x}$ denote the horizontal outer boundaries of the stance and swing feet, respectively. In (6), $\delta_1, \delta_2 \geq 0$ are relaxation terms that can be tuned to expand the stability margin to tolerate natural gait variability and individual stabilization strategies. Additionally, these terms are also used to approximate the anterior/posterior foot positions for the simplified point-feet model used during experiments (to be specified in Sec. V-A). The proposed stability indicator treats the gait stability as the swing leg's ability to catch an unstable body (see Fig. 1 for illustration), since during steady locomotion the swing leg is positioned to arrest a developing fall at the next foot contact [25]. Finally, we define a relative-degree one CBF that considers both s and its derivative, *i.e.*,

$$h = \gamma_1 s + \gamma_2 \dot{s} + c, \tag{7}$$

where $\gamma_1, \gamma_2 > 0$ control the contribution of s and $\dot{s}$ to h [26], $c \geq 0$ is a relaxation term that allows the user to approach or slightly exceed the safe set and thus provide flexibility to user-specific stabilization strategies. We can see from (6) and (7) that h has a similar form to XCoM, which is expressed as $\text{CoM}_x + \dot{\text{CoM}}_x/\omega_0$ with ω_0 being the eigenfrequency [27], but we modify it by replacing the raw CoM term with a CoM-based stability indicator and adding small, tunable margins to reduce sensitivity to normal gait variability and avoid unnecessary corrective actions that may interfere with the user's voluntary motion.

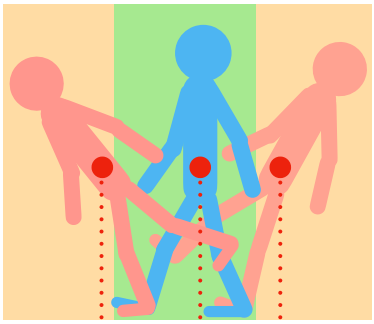

Fig. 1. Illustration of the safety indicator in (6). The green/yellow areas represent the stability-safe/unstable ranges of the indicator, and the red dot denotes the CoM position.

With the CBF defined in (7), we incorporate it into an quadratic programming (QP) to determine SAC control law

as

$$\begin{aligned}\min_{u} \quad & u^\top W u \\ \text{s.t.} \quad & \frac{\partial h}{\partial q}\dot{q} + \frac{\partial h}{\partial \dot{q}} M^{-1}(-C\dot{q} - N - A^\top \lambda + \tau_{\text{hum}} + Bu \\ & \qquad + J^\top F_{\text{perturb}}) \geq -\alpha(h), \end{aligned} \tag{8}$$

where W is a diagonal, positive definite weight matrix, and $\alpha(\cdot)$ is an extended class $\mathcal{K}_\infty$ function. Note that the proposed control strategy not only considers the geometric relations between CoM and foot positions, it also incorporates system dynamics with the user's voluntary motion τ_{hum}, whose estimation will be introduced in Sec. III-B.

B. Human Joint Torque Estimation via NDO

Solving (8) requires the knowledge of human joint torque τ_{hum}, which can be hard to measure directly in practice. To address this, we propose a novel NDO [28] to estimate a modified term of human input $M^{-1}(I - A^\top \check{\lambda})\tau_{\text{hum}}$ based on human joint kinematics through the Euler-Lagrange dynamics (1). Rather than estimating τ_{hum} directly, we estimate this modified form because it appears explicitly in (8) and avoids sensitivity to potential small eigenvalues from M. Left multiplying by M^{-1} on both sides of (1) yields

$$\ddot{q} + M^{-1}(C\dot{q} + N + A^\top \hat{\lambda}) = M^{-1}B_\lambda u + z. \tag{9}$$

Here, $z = M^{-1}(I - A^\top \check{\lambda})\tau_{\text{hum}}$ represents the "disturbance" term to be estimated, and $B_\lambda = (I - A^\top \check{\lambda})B$. Note that when an external perturbation is present, this term would consist of both human input and the external perturbation forces, *i.e.*, $z = M^{-1}[(I - A^\top \check{\lambda})\tau_{\text{hum}} + J^\top F_{\text{perturb}}]$. Rewriting (9) as

$$z = \ddot{q} + M^{-1}C\dot{q} + M^{-1}N + M^{-1}A^\top \hat{\lambda} - M^{-1}B_\lambda u \tag{10}$$

and defining $\hat{z}$ to be the estimate of z, we have:

$$\begin{aligned}\dot{\hat{z}} &= L(z - \hat{z}) \\ &= -L\hat{z} + L[\ddot{q} + M^{-1}(C\dot{q} + N + A^\top \hat{\lambda} - B_\lambda u)], \end{aligned} \tag{11}$$

where $L \in \mathbb{R}^{n \times n}$ is a diagonal, positive definite matrix to be designed. During implementation, $\hat{z}$ can be numerically updated as $\hat{z}_{k+1} = \hat{z}_k + \Delta t\, l(\hat{z}_k, q, \dot{q}, \ddot{q}, u)$, where Δt is the sampling period and $l(\hat{z}_k, q, \dot{q}, \ddot{q}, u)$ represents the right-hand-side of (11) evaluated at the current states and control input. Assuming the changing rate of modified human input $\dot{z}$ is bounded [25], we can guarantee that the estimation error $e = z - \hat{z}$ is uniformly ultimately bounded [29].

Remark 1. *Building on the NDO formulation in* (9)*, we rewrite* (1) *by separating the nominal dynamics, control input, and NDO-estimated disturbance terms:*

$$\begin{aligned}\dot{x} &= \begin{bmatrix} \dot{q} \\ -M^{-1}(C\dot{q} + N + A^\top \hat{\lambda}) \end{bmatrix} + \begin{bmatrix} 0 \\ M^{-1}B_\lambda \end{bmatrix} u + \begin{bmatrix} 0 \\ \hat{z} + e \end{bmatrix} \\ &:= \begin{bmatrix} \dot{q} \\ -M^{-1}(C\dot{q} + N + A^\top \hat{\lambda}) \end{bmatrix} + \begin{bmatrix} 0 \\ M^{-1}B_\lambda \end{bmatrix} u + d + d_{\text{err}}, \end{aligned}$$

where $e = z - \hat{z}$ is the NDO estimation error, $d = (0^\top, \hat{z}^\top)^\top$, and $d_{\text{err}} = (0^\top, e^\top)^\top$. Therefore, the time derivative of h becomes

$$\dot{h} = L_f h + L_g h u + L_d h + L_{d_{\text{err}}} h. \tag{12}$$

The QP in (8) *enforces the nominal CBF condition*

$$L_f h + L_g h u + L_d h \geq -\alpha(h), \tag{13}$$

while the actual closed-loop dynamics satisfy

$$L_f h + L_g h u + L_d h + L_{d_{\text{err}}} h \geq -\alpha(h) + L_{d_{\text{err}}} h. \tag{14}$$

Since h depends on CoM position and velocity, $\frac{\partial h}{\partial \dot{q}}$ is bounded. For sufficiently large time,

$$\begin{aligned} L_{d_{\text{err}}} h &= \begin{bmatrix} \frac{\partial h}{\partial q} & \frac{\partial h}{\partial \dot{q}} \end{bmatrix} \begin{bmatrix} 0 \\ e \end{bmatrix} \\ &= \left\langle \frac{\partial h}{\partial \dot{q}}, e \right\rangle \geq -\bar{h}_q \cdot \bar{e}, \end{aligned} \tag{15}$$

where $\bar{e}$ is e's ultimate bound. Substituting (15) *into* (14) *yields*

$$L_f h + L_g h u + L_d h + L_{d_{\text{err}}} h \geq -\alpha(h) - \bar{h}_q \cdot \bar{e}. \tag{16}$$

Therefore, the bounded NDO error introduces a bounded slack term in the CBF condition. As a result, exact forward invariance of the original safe set is not guaranteed under the true closed-loop dynamics [23], but the deviation from the nominal condition remains bounded. The relaxation term c in (7) *can be tuned to enforce earlier intervention before the true boundary is reached, improving robustness to estimation error. A detailed invariance analysis is left for future work.*

IV. Bilateral Hip Exoskeleton System

To evaluate the performance of our proposed SAC, we conducted human-subject experiments on a bilateral, powered hip exoskeleton (SportsMate 5, Enhanced Power Technology Co., Ltd., Shenzhen, China, Fig. 2, left) equipped with externally mounted inertial measurement units (IMUs) and a Raspberry Pi board (Fig. 2, right). We selected SportsMate 5 for experiments because the hip joint plays a key role in recovering from destabilizing events such as slips [30], making hip assistance particularly relevant for restoring gait stability. At the same time, the lightweight design and highly backdrivable actuators of the exoskeleton align with our control objective of providing stability augmentation while preserving voluntary human responses. In this section, we present the exoskeleton hardware, the external sensors used for kinematics measurements, and the overall control architecture.

A. SportsMate 5 Exoskeleton

SportsMate 5 has two brushless DC motors (ER-Motor 5008, Enhanced Power Technology Co., Ltd., Shenzhen, China). Each motor is designed for high backdrivability in a compact size (50 × 18 mm), with a high torque density of 21.4 Nm/kg, and a low rotor inertia of 0.09 kg·cm^2. Each motor can deliver 7.5 Nm rated torque and 22.5 Nm peak torque. The torque is transmitted through a quasi-direct drivetrain that combines planetary gears and belts (25:1 gear ratio) that reduces mechanical damping and friction. The system achieves a low backdrive torque of 0.096 Nm, with a backdrivability ratio (ratio of rated torque to backdrive torque) of 78.4 to encourage voluntary human movements. The actuator system enables current regulation at 400 Hz through a GD32F303RE

microprocessor (ARM Cortex-M4, 120 MHz, 512 kB ROM, 64 kB RAM) along with two 14-bit single-turn absolute magnetic joint encoders and current sensors. The system is powered by a 3200 mAh onboard lithium battery.

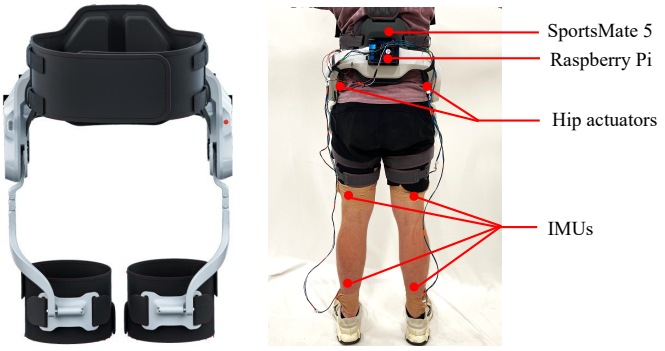

Fig. 2. Left: The SportsMate 5 exoskeleton. Right: A subject wearing SportsMate 5 with externally mounted IMUs and a Raspberry Pi.

B. Human Kinematics Measurements

We measured joint kinematics via four IMUs (NGIMU, x-io Technologies Ltd., Bristol, UK) placed at the individual's thighs and shanks to collect ankle, knee and hip orientations at 200 Hz. The IMUs used the built-in Attitude and Heading Reference System fusion algorithm [31] for signal smoothing. The measurements were then transmitted to a Raspberry Pi 4B (8GB LPDDR4-3200 SDRAM, Cortex-A72 64-bit SoC, 1.8 GHz) over UART. Finally, we used these joint angles along with their numerical derivatives for NDO and SAC calculation. During calculation, we smoothed the acceleration with a 71-sample moving average filter [32].

C. Control Architecture

The overall control structure consists of two loops: a high-level loop that handles communication and real-time computation, and a low-level loop that implements torque control (Fig. 3). We used a Raspberry Pi to communicate with the IMUs and the SportsMate 5, perform real-time human input estimation using an NDO, and compute the control input in (8) using an open-source, lightweight solver Operator Splitting Quadratic Program (OSQP) [33]. The resulting torque command is transmitted to the SportsMate 5 via UART, where the embedded motor driver (ER-Driver) regulates actuator current to realize the desired torque through a torque controller with a torque constant of 0.083 Nm/A. Although the control algorithm can run at 300 Hz on the Raspberry Pi, the update rate was limited to 150 Hz during experiments to match the SportsMate 5 communication frequency.

V. Experimental Study

A. Experimental Model

Given that ankle joints are relatively less dominant during stability recovery [30] and that the SportsMate 5 does not directly assist the ankle joints, we adopted a simplified 4-DoF biped model in the experiments (Fig. 4) to realize

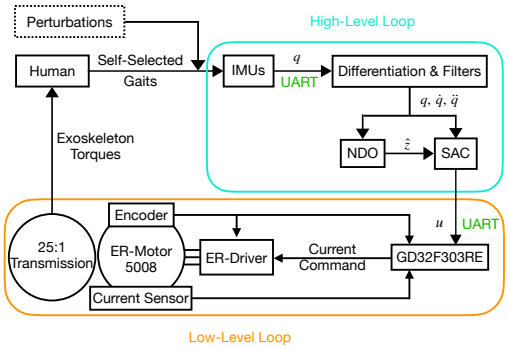

Fig. 3. Overall structure of the exoskeleton control system.

a manageable computational burden on the Raspberry Pi. The configuration vector of this model is selected as $q = (\phi, \theta_{\mathrm{k}}, \theta_{\mathrm{h}}, \theta_{\mathrm{sk}})^\top \in \mathbb{R}^4$, where ϕ represents the global orientation of stance shank, and θ_{i}, $i \in \{\mathrm{k}, \mathrm{h}, \mathrm{sk}\}$ denote the relative angles of stance knee, hip, and swing knee, respectively. All inertial parameters are estimated using the methods in [34]. The experimental model is established based on an inertial reference frame (IRF) fixed at the user's stance foot. To accommodate the IRF shifts during stance leg switching, we maintained two identical 4-DoF models, each anchored to one foot. During experiments, the model corresponding to the current stance leg is used to compute u, which is then applied to the ipsilateral hip actuator. We split u equally between the two actuators, motivated by the approximately symmetric hip torque profiles observed during steady-state walking [34] and evidence that recovery strategies are largely invariant to perturbation side [35]. Our experimental results further show that this equal torque distribution helps stabilize the stance leg while advancing the swing leg during perturbations to reduce their muscle activities. During experiments, we saturated the actuator torques at ± 15 Nm to avoid excessive torques.

Since the model assumes no-slip stance-foot contact, the constraint force λ can be eliminated in (1), yielding $B_\lambda = B$ in (9) [36]. During perturbed situations such as slips, this assumption is transiently violated. Since such violation is brief, we retained this simplified model for control calculation and treated the foot slip as transient unmodeled disturbances, which can be estimated via the NDO.

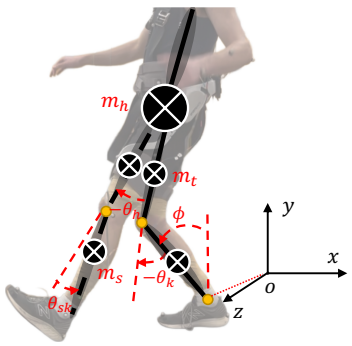

Fig. 4. A representative backward slipping configuration of a subject and the corresponding 4-DoF biped model used for the experiments, where the upper-body and hip are lumped into a single point mass.

B. Experimental Protocol

Four non-disabled subjects (4 males, s1–s4, age: 26.8 ± 5.9, mass: 80.4 ± 15.6 kg, height: 1.82 ± 0.09 m) were recruited for the experiments, where a similar sample size can be found in previous studies [37]. The experimental protocol was approved by the Institutional Review Board of the author's affiliated institution, and written informed consent was obtained prior to experiments. At the beginning of the experiments, the subjects were asked to walk on the treadmill at various speeds (0.8, 1.0, 1.2 m/s) for 30 s under passive mode (PAS, exoskeleton worn with actuators off) for data collection and subject-specific parameter tuning (δ_1, δ_2, γ_1, γ_2, and c) for SAC. Parameters were tuned during steady-state walking so that the controller remained effectively inactive and kept unchanged for the remainder of experiments.

After level-ground walking trials, each subject completed two sessions, *i.e.*, forward leaning (FL)/backward leaning (BL), and forward slipping (FS)/backward slipping (BS), where their conditions are summarized in Fig. 5. For leaning trials, the subject stood still while the treadmill started to slowly move to induce a gradual forward (FL) or backward (BL) lean. The subject was instructed to keep their feet in place until a corrective response had to be made when stability was compromised. To ensure consistency across subjects and trials, subjects were instructed to initiate the recovery step with their right legs. For slipping trials, we approximated slip-like perturbations by triggering a sudden anteroposterior treadmill belt acceleration/deceleration during early stance after a pseudo-random number of steady-state steps [38]. The detailed perturbation information can be found in Fig. 5. Note that we used two perturbation parameter settings (belt accelerations and durations) for BS trials to accommodate between-subject differences in body size, generating noticeable gait changes while avoiding excessive instability to ensure subject safety. The order of all slip trials was pseudo-randomized to prevent anticipation and user adaptation.

Throughout experiments, we chose $\alpha(h) = 0.1h^3$ from pilot trials, aiming to generate rapid control input response for unstable postures, set W as an identity matrix, and $L = 100 \cdot I_{4\times4}$ in the NDO to ensure rapid tracking of Winter's hip torque profile [34] from simulation studies [29]. During slipping trials, we additionally implemented a whole-body angular momentum regulation controller (MRC) [29] for comparison with the proposed SAC assistance. We selected MRC parameters to enable continuous regulation of whole-body angular momentum of individuals, which is a common gait stability metric, to mitigate perturbation-induced gait deviations. Throughout experiments, the subjects wore an overhead harness to ensure safety without obstructing data collection.

For the leaning trials, we define the perturbation interval from the moment the subjects started the reactive stepping motion, *i.e.*, moving their legs in response to the unstable posture, to the subsequent foot strike of the stepping foot, at which a stable configuration is re-established. For slipping trials, we define the perturbation interval as the period from the heel strike right before the treadmill acceleration, to the moment of the second heel strike of the same foot following the acceleration, by which time stable gait is re-established as indicated by the WBAM analysis.

C. Muscle Activities and Kinematics

To evaluate the performance of the proposed control strategy, we measured the subjects' muscle activities via electromyographic (EMG) sensors (Trigno Sensor, Delsys Inc., MA, USA). We recorded Rectus Femoris (RF), Biceps Femoris (BF), Gluteus Medius (GMed), Gluteus Maximus (GMax), Tibialis Anterior (TA), and Soleus (SOL) at 2000 Hz, where RF primarily acts as a hip flexor, BF as a primary hip extensor, GMed as the primary hip abductor with a secondary role in hip extension/stabilization, GMax as a major hip extensor, TA as an ankle dorsiflexor, and SOL as a primary ankle plantarflexor [39]. EMG data was first filtered by a 4th-order band-pass filter with a 20-500 Hz passband and rectified, and then filtered by a low-pass filter with 6 Hz cutoff frequency. The EMG data was then normalized with respect to the maximum peak EMG values throughout steady-state walking trials, thereby converting the signals to a percentage of the peak filtered EMG values. We also recorded the subjects' body movements via a motion capture system (Vicon, Oxford, UK). We applied a modified Plug-in-Gait Full Body model [40] with a total of 30 retroreflective markers. The 3D marker trajectories were collected at 100 Hz and used to calculate the human joint kinematics in OpenSim with a scaled musculoskeletal model (22 rigid bodies, 37 DoFs [41]). Finally, we calculated the subjects' WBAM with the resulting kinematic data.

VI. Results & Discussion

In this section, we present estimated human joint torques, exoskeleton torques, stability indicator values, muscle activation, and WBAM results in Figs. 6 to 10. In all figures, 0% of the gait cycle represents the onset of stance leg heel strike, and 100% represents the next heel strike of the same leg. For leaning trials, 0% and 100% denote the start and end of the perturbation intervals, respectively. Positive/negative values of torques denote hip extension/flexion, respectively. A total of 10 leaning and 12 slipping trials were collected with SAC. For analysis, fixed subsets (5 leaning, 6 slipping) meeting pre-defined quality criteria (complete EMG/marker data and correct actuator execution) were selected to balance sample sizes. The same criteria were applied across all subjects and conditions and did not affect the reported trends.

A. Nonlinear Disturbance Observer

We demonstrate the performance of the proposed NDO on hip torque estimation in Fig. 6. As shown in the left graph, the estimated hip torque closely matches the waveform and magnitude reported in Winter's normative gait dataset [34], showcasing the feasibility of the proposed NDO, even with the simplified 4-DoF experimental model (Fig. 4).

To further evaluate the NDO, we estimated joint torques from the kinematics in [42] using an 8-DoF human-exoskeleton model (see [29] for details) and compared them with the biological torques reported in [42]. Subject-specific

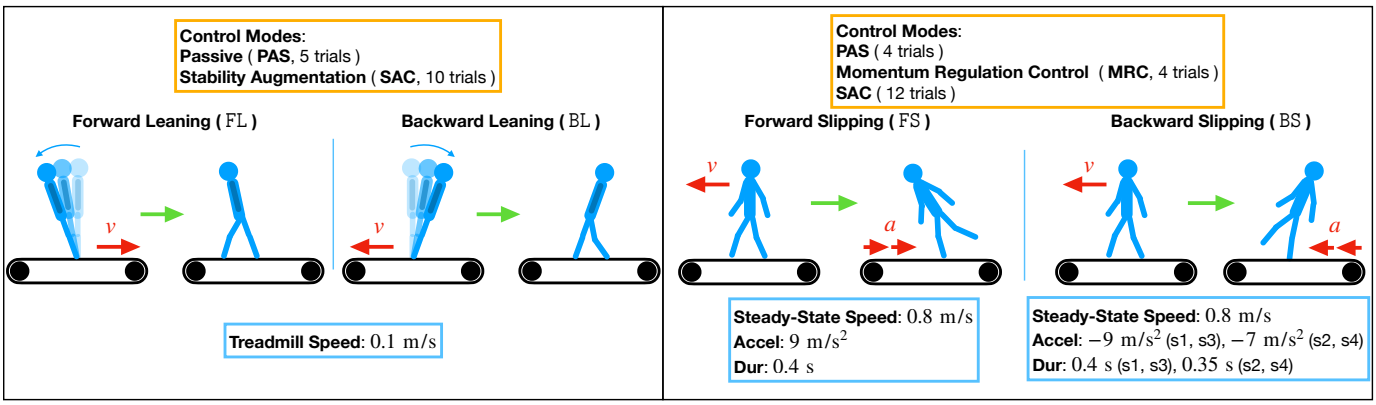

Fig. 5. Summary of experimental setup and conditions.

limb length, segment mass, and moments of inertia were approximated using the scaling procedures in [34]. Also, to account for parametric mismatch in the human-exoskeleton model, we introduced a 10% parametric uncertainty during torque estimation. Even under these uncertainties, the estimated hip torques remain close to the reference torques (Fig. 6, right), with estimation errors staying within an acceptable range throughout most of the gait cycle. The discontinuity near 50% gait corresponds to the stance-leg transition, during which the IRF changes.

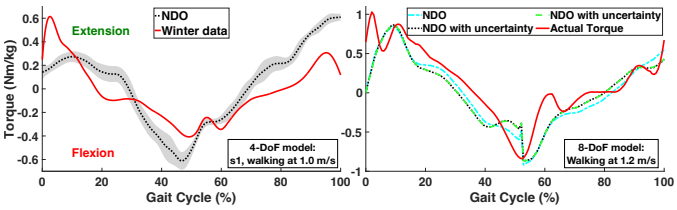

Fig. 6. Mean $\pm$ 1 $\cdot$ SD of NDO estimated hip torques compared with Winter's dataset (left) and the biological hip torques from [42] in the presence of random, 10% parameter uncertainties (right).

In Fig. 6 (right), the estimation yielded a root-mean-square error (RMSE) ranging from 0.20 to 0.24 Nm/kg, and the coefficient of determination (R^2) ranging from 0.60 to 0.84, which are consistent with the accuracy reported by existing estimation methods [43], suggesting that the NDO can estimate hip torques with reasonable accuracy.

B. Exoskeleton Torques & Stability Indicator

Sample exoskeleton torques along with the corresponding s values are shown in Fig. 7. The torques remained near zero during stable postures and increased rapidly following the onset of instability caused by excessive leaning angles or the onset of slip perturbations, which are successfully detected by the proposed stability indicator (with s approaching zero or becoming negative) in all scenarios. Notably, the proposed controller generated distinct torque profiles and directions across perturbation conditions without pre-specifying torque waveforms, suggesting good adaptability to different perturbation scenarios.

During leaning trials, the delay between exoskeleton torque onset and the unstable postures ($s < 0$, highlighted by the blue box in Fig. 7) arises from the relaxation term in (7), which keeps h positive under mildly unstable conditions. This allows small deviations from the nominal safe set, allowing voluntary responses and user-specific stabilization strategies. In contrast, during slipping trials, the exoskeleton torque was activated before s became negative, as highlighted by the green box in Fig. 7. This earlier onset is due to two features of the CBF design. First, $\dot{s}$ in (7) captures the evolution of stability, so rapid perturbations can drive the system toward an unsafe condition even before s becomes negative. Second, the selected $\alpha(h)$ in (8) allows $\dot{h}$ to be slightly negative when h is positive but close to zero. As a result, when human effort alone is insufficient during large slip perturbations, the controller provides torques preemptively to prevent potential gait instability. Together, these mechanisms enable SAC to assist before an unstable posture fully develops, which is often required as shown in previous studies [11].

C. EMG & Muscular Efforts

The ensemble-averaged normalized EMG patterns for leaning trials are shown in Fig. 8. Overall, all recorded muscles show consistently lower activities with SAC compared to PAS, indicating that the proposed control can effectively offload the subjects' muscle activities during recovery. Specifically, during FL trials, the subject flexed the right hip joint (swing side) and thus moved the right leg forward to complete a step and catch the forward-falling body. Accordingly, the right RF, a hip flexor, became highly active, and the right-hip flexion exoskeleton torque (Fig. 7) reduced the biological hip flexion demand, thereby offloading the right RF activation [39]. In the meantime, flexion exoskeleton torque could accelerate the swing leg and reduce the urgency in toe-clearance and foot-placement corrections, and thus decreased the muscle activity of right TA [44]. In contrast, the corresponding left-hip (stance side) extension exoskeleton torques helped prevent the pelvis and trunk from pitching forward to reduce the required stance hip extensor effort, leading to a large decrease in the left GMax. Moreover, according to subjects' feedback, the left-hip extension exoskeleton torque helped to stabilize their stance legs, and thus could result in reduced demand of stabilization with GMed and SOL [45], [46]. Similarly, during BL trials, the right-hip extension exoskeleton torque reduced the need for

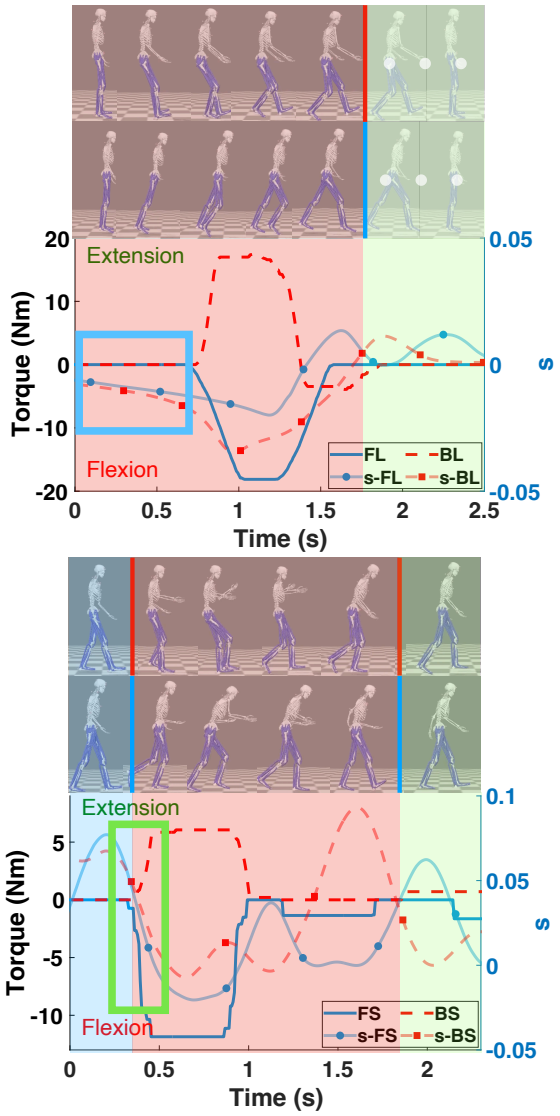

Fig. 7. Sample swing leg exoskeleton torques of s1 along with stability indicator value (s) and related postures during leaning (top) and slipping trials (bottom). Blue/red/green shaded areas indicate the pre-, during-, and post-perturbation intervals, respectively.

right hip extensor during recovery step, resulting in reduced activation of right RF, BF, and GMax compared with PAS.

For slipping trials, subjects exhibited varying stability recovery strategies, leading to trial- and subject-specific variations in EMG waveforms. To better quantify the effect of the proposed control on muscle activities, we present the average normalized integrated EMG (iEMG) across subjects and trials in Fig. 9. Overall, compared with PAS and MRC modes, SAC yielded lower iEMG values in almost all recorded muscles during `FS` and `BS` trials, suggesting that SAC can effectively offload the subjects' muscle activities during slip perturbations. In particular, SAC reduced iEMG in hip extensors and flexors (RF, GMax, and BF), indicating direct offloading of the hip demands needed for transient rapid stability recovery. The reduced GMed activity further highlights decreased hip stabilization effort [45].

Moreover, similar to leaning trials, the reduced TA and SOL iEMG could indicate reduced reliance on ankle-based stabilization compensation during perturbations [47]. In contrast, MRC generally increased iEMG across muscles, indicating that this control strategy designed for stable walking may not be able to naturally translate to effective stability recovery under perturbations. Therefore, these results suggest that SAC not only directly reduces activities of hip-related muscles, but could also have indirect benefits on the distal muscles such as TA and SOL.

Quantitatively, we defined the subject muscular effort as the average normalized iEMG over the perturbation interval of all recorded muscles across all trials [48]. We then calculated the ensemble-averaged muscle effort across all 4 subjects, *i.e.*,

$$\text{Effort} = \frac{1}{4}\cdot\frac{1}{12}\frac{1}{n_{\text{mode}}}\sum_{k}\sum_{t}\sum_{i}\frac{\text{iEMG}_{i,t,k}}{\text{EMG}_{\text{max},i,k}}, \qquad (17)$$

where n_{mode} denotes the number of trials within a control mode, $\text{iEMG}_{i,t,k}$ is the iEMG of muscle i for subject k in trial t, with $i \in \{\text{RF}, \text{BF}, \text{GMed}, \text{GMax}, \text{TA}, \text{SOL}\}$ for both legs, and $\text{EMG}_{\text{max},i,k}$ denotes the maximum EMG value of subject k's muscle i during steady-state walking. The results are shown in Figs. 9 and 8. On average, compared to PAS, SAC reduced subjects' muscle efforts by 32.16%, 49.34%, 9.41%, and 31.85% in `FL`, `BL`, `FS`, and `BS` trials, respectively. Overall, these results indicate that SAC can consistently offload muscle activities during stability recovery under both quasi-static (leaning) and dynamic (slip) perturbations.

D. Whole-Body Angular Momentum

WBAM is often used to quantify gait stability [49] during locomotion. Unstable or perturbed gaits tend to result in larger WBAM deviations compared to steady-state walking [50]. Therefore, we report the individual and ensemble-averaged sagittal-plane WBAM of all subjects in Figs. 10 and 11, respectively. Across all subjects, slip perturbations resulted in noticeable WBAM deviations relative to steady-state walking, followed by a recovery toward steady oscillations. Compared with PAS and MRC, SAC consistently reduced the maximum WBAM deviations in both `FS` and `BS` trials, indicating that SAC effectively improves gait stability during perturbed walking. Quantitatively, compared with PAS, SAC reduced the peak-to-peak WBAM by 6.43% and 11.69% on average during `FS` and `BS` trials, respectively (Fig. 11). The larger reduction observed in `BS` trials could reflect SAC's effectiveness under more challenging and demanding conditions based on subjects' feedback. In contrast, PAS and MRC tended to result in larger WBAM peaks or prolonged deviations during the post-perturbation phase, suggesting less effective stability recovery performance compared with SAC.

To further evaluate the proposed control strategy in gait stability recovery, we computed the mean WBAM-based recovery time (Fig. 10), following the general "return-to-baseline and remain" concept in [51]. For each subject, we first identified the time of the peak WBAM and constructed a steady-state recovery band from the final portion of the perturbation interval using its median and a robust variability estimate. Specifically, we computed a median absolute deviation from the median (MAD)-based robust standard deviation $\text{SD}_{\text{rob}} =$

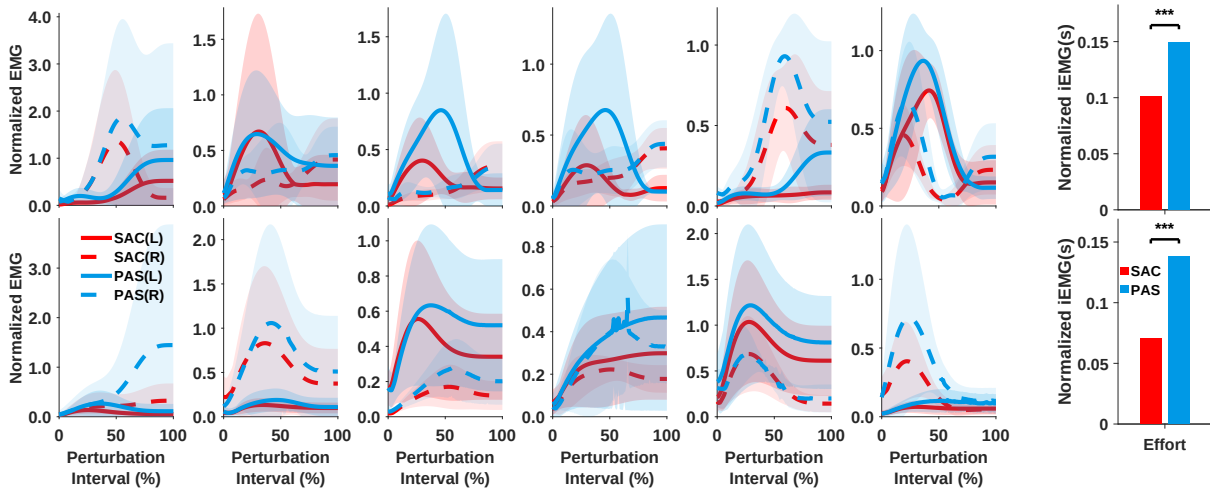

Fig. 8. Ensemble-averaged normalized EMG (mean $\pm$ 1 $\cdot$ SD) for subjects s1 - s4. Solid and dashed lines denote muscles on the left and right muscles, respectively. The top and bottom rows correspond to FL and BL, with columns indicating RF, BF, GMed, GMax, TA, SOL, and the muscle efforts (left to right). Muscular effort was analyzed using mixed-effects analysis of variance (ANOVA) ($***$ indicates P $\leq$ 0.001). Spikes in GMax under BL reflect noise artifacts.

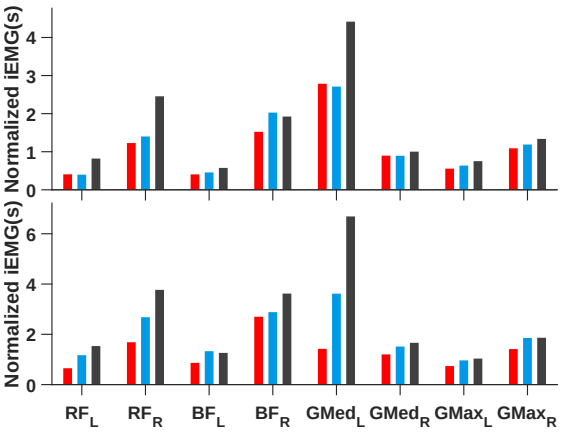

(a) Proximal hip muscles (top: FS, bottom: BS)

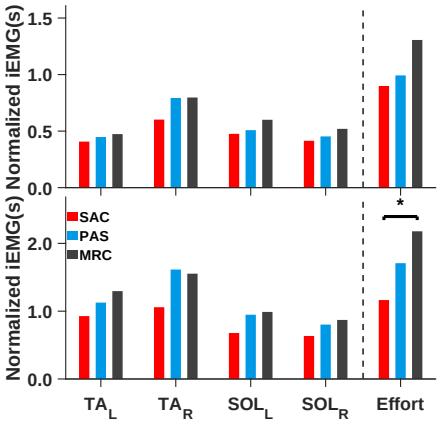

(b) Distal muscles and effort (top: FS, bottom: BS)

Fig. 9. Ensemble-averaged muscle activities and efforts, $*$ indicates P $\leq$ 0.05.

$\pm$ 1.4826 $\cdot$ MAD. The recovery time was defined as the earliest time after the peak at which WBAM re-entered the recovery band (median $\pm$ 2.5 $\cdot$ $\mathrm{SD_{rob}}$) and remained within this range through the end of the interval, allowing only rare, brief out-of-band deviations. In general, shorter recovery time represents faster recovery to steady-state walking after perturbation. In Fig. 10, SAC reduced the mean recovery time in most conditions. The MRC, however, reduced the mean recovery time in some conditions, but showed less consistent stability recovery performance across metrics. Together with peak-to-peak WBAM and muscle activity, benefits of MRC seem more condition-dependent.

VII. Conclusion

This paper presents an SAC to augment gait stability under unstable gaits or external perturbations. The proposed approach first defines a CoM-based stability indicator, and enforces it to remain within a safe range defined over position and velocity using CBFs. The proposed approach does not prescribe reference kinematics, and assistance is only triggered when gait stability is approaching or exceeding the safe range, thus allowing human voluntary motion while providing proactive assistance. Moreover, to explicitly account for human input, we propose an NDO to estimate human joint torques in real time. Experimental results with four non-disabled subjects performing quasi-static leaning tasks and steady-state walking under slip perturbations validate the effectiveness of the proposed method in reducing muscular efforts, lowering perturbation-induced peak-to-peak WBAM, and shortening the mean recovery time. Future work will integrate SAC with existing controllers for steady, nominal walking to provide seamless assistance across both stable and unstable gait conditions.

References

[1] S. L. James, L. R. Lucchesi, C. Bisignano, C. D. Castle, Z. V. Dingels, J. T. Fox, E. B. Hamilton, N. J. Henry, K. J. Krohn, Z. Liu *et al.*, "The global burden of falls: global, regional and national estimates of morbidity and mortality from the global burden of disease study 2017," *Inj. Prev.*, vol. 26, no. Suppl 2, pp. i3–i11, 2020.

[2] A. B. Peterson and K. E. Thomas, "Incidence of nonfatal traumatic brain injury–related hospitalizations—united states, 2018," *MMWR. Morbidity and mortality weekly report*, vol. 70, 2021.

[3] Y. Wang, T. Bhatt, X. Liu, S. Wang, A. Lee, E. Wang, and Y.-C. C. Pai, "Can treadmill-slip perturbation training reduce immediate risk of over-ground-slip induced fall among community-dwelling older adults?" *J. Biomech.*, vol. 84, pp. 58–66, 2019.

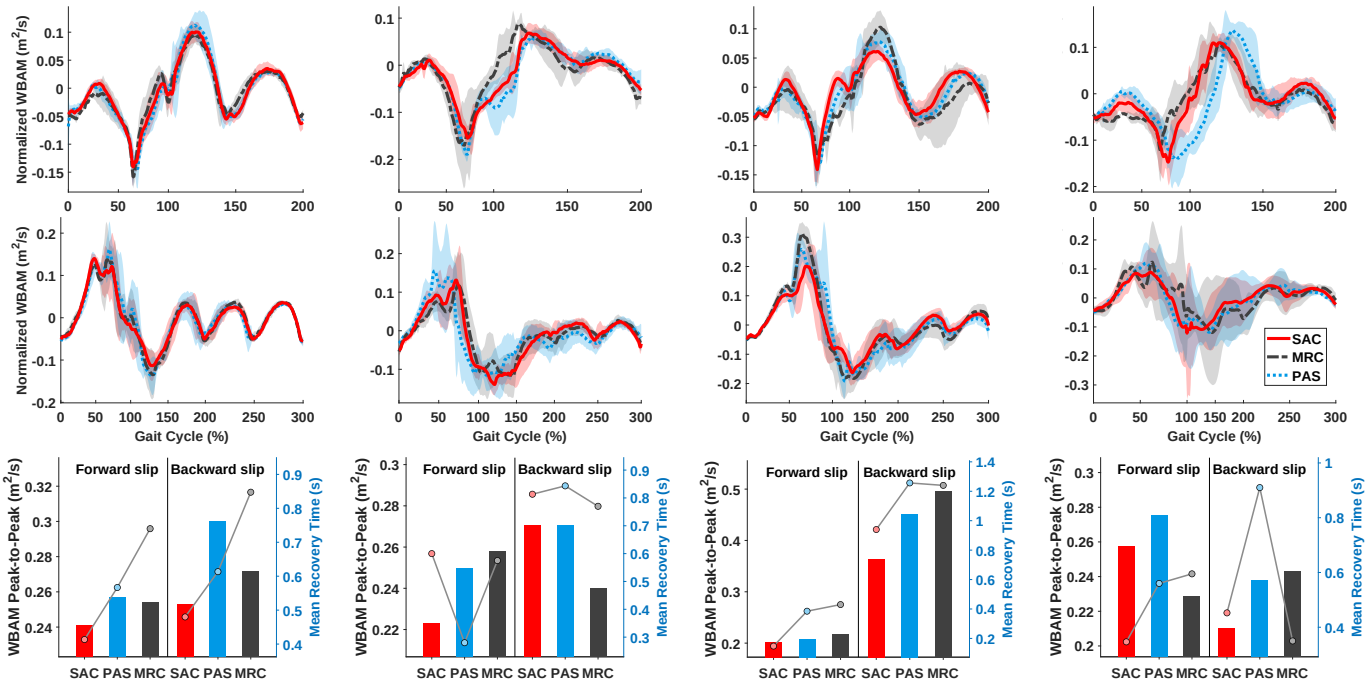

Fig. 10. Mean $\pm$ 1$\cdot$ SD individual sagittal WBAM of s1 - s4 (left to right) in FS (top), BS (middle), and bar plots of average peak-to-peak WBAM with recovery time (bottom).

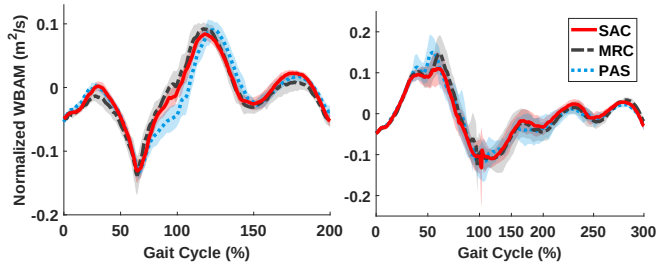

Fig. 11. Mean $\pm$ 1 $\cdot$ SD sagittal WBAM across all subjects in FS (left) and BS (right) trials.

[4] M. Sehgal, J. Jacobs, and W. S. Biggs, "Mobility assistive device use in older adults," *Am. Fam. Physician*, vol. 103, no. 12, pp. 737–744, 2021.

[5] A. M. Korall, F. Feldman, Y. Yang, I. D. Cameron, P.-M. Leung, J. Sims-Gould, and S. N. Robinovitch, "Effectiveness of hip protectors to reduce risk for hip fracture from falls in long-term care," *Journal of the American Medical Directors Association*, vol. 20, no. 11, pp. 1397–1403, 2019.

[6] D. J. Haight, E. R. Esposito, and J. M. Wilken, "Biomechanics of uphill walking using custom ankle-foot orthoses of three different stiffnesses," *Gait Posture*, vol. 41, no. 3, pp. 750–756, 2015.

[7] G. Lv, H. Zhu, and R. D. Gregg, "On the design and control of highly backdrivable lower-limb exoskeletons: A discussion of past and ongoing work," *IEEE Control Syst. Mag.*, vol. 38, no. 6, pp. 88–113, 2018.

[8] V. Monaco, P. Tropea, F. Aprigliano, D. Martelli, A. Parri, M. Cortese, R. Molino-Lova, N. Vitiello, and S. Micera, "An ecologically-controlled exoskeleton can improve balance recovery after slippage," *Sci. Rep.*, vol. 7, no. 1, p. 46721, 2017.

[9] M. Afschrift, E. Van Asseldonk, M. Van Mierlo, C. Bayon, A. Keemink, L. D'Hondt, H. Van Der Kooij, and F. De Groote, "Assisting walking balance using a bio-inspired exoskeleton controller," *J. Neuroeng. Rehabil.*, vol. 20, no. 1, p. 82, 2023.

[10] T. J. Ellmers, M. R. Wilson, E. C. Kal, and W. R. Young, "The perceived control model of falling: developing a unified framework to understand and assess maladaptive fear of falling," *Age Ageing*, vol. 52, no. 7, p. afad093, 2023.

[11] O. N. Beck, M. K. Shepherd, R. Rastogi, G. Martino, L. H. Ting, and G. S. Sawicki, "Exoskeletons need to react faster than physiological responses to improve standing balance," *Sci. Robot.*, vol. 8, no. 75, p. eadf1080, 2023.

[12] S. Luo, G. Androwis, S. Adamovich, E. Nunez, H. Su, and X. Zhou, "Robust walking control of a lower limb rehabilitation exoskeleton coupled with a musculoskeletal model via deep reinforcement learning," *J. Neuroeng. Rehabil.*, vol. 20, no. 1, p. 34, 2023.

[13] J. Pratt, J. Carff, S. Drakunov, and A. Goswami, "Capture point: A step toward humanoid push recovery," in *IEEE-RAS Int. Conf. Humanoid Robots*, 2006, pp. 200–207.

[14] M. Deng, Z. Ma, Y. Wang, H. Wang, Y. Zhao, Q. Wei, W. Yang, and C. Yang, "Fall preventive gait trajectory planning of a lower limb rehabilitation exoskeleton based on capture point theory," *Front. Inf. Technol. Electron. Eng.*, vol. 20, pp. 1322–1330, 2019.

[15] C. Zhu and J. Yi, "Knee exoskeleton-enabled balance control of human walking gait with unexpected foot slip," *Robot. Autom. Lett.*, vol. 8, no. 11, pp. 7751–7758, 2023.

[16] A. Vallinas, A. Keemink, C. Bayón, E. van Asseldonk, and H. van der Kooij, "Momentum-based balance control of a lower-limb exoskeleton during stance," in *Int. Conf. Rehabil. Robot.* IEEE, 2023, pp. 1–6.

[17] T. Zhang, M. Tran, and H. H. Huang, "Nrel-exo: A 4-dofs wearable hip exoskeleton for walking and balance assistance in locomotion," in *Int. Conf. Intell. Robots Syst.* IEEE, 2017, pp. 508–513.

[18] Z. Li, "Comparison between safety methods control barrier function vs. reachability analysis," *arXiv preprint arXiv:2106.13176*, 2021.

[19] T. Gurriet, A. Singletary, J. Reher, L. Ciarletta, E. Feron, and A. Ames, "Towards a framework for realizable safety critical control through active set invariance," in *IEEE Int. Conf. Cyber-Phys. Syst.*, 2018, pp. 98–106.

[20] A. Agrawal and K. Sreenath, "Discrete control barrier functions for safety-critical control of discrete systems with application to bipedal robot navigation." in *Robot. Sci. Syst.*, vol. 13. Cambridge, MA, USA, 2017, pp. 1–10.

[21] Y. Zhou, J. Cheng, B. Chen, J. Zhou, K. Yue, and Z. Wang, "Cbf-based constrained optimization for safe and adaptive cpg gait planning in rehabilitation robots," in *Chin. Control Conf.* IEEE, 2025, pp. 5095–5100.

[22] R. M. Murray, Z. Li, and S. S. Sastry, *A Mathematical Introduction to Robotic Manipulation*. NW Boca Raton, FL: CRC press, 2017.

[23] A. D. Ames, S. Coogan, M. Egerstedt, G. Notomista, K. Sreenath, and P. Tabuada, "Control barrier functions: Theory and Applications," in *Eur. Control Conf.* IEEE, 2019, pp. 3420–3431.

[24] C. Curtze, T. J. Buurke, and C. McCrum, "Notes on the margin of stability," *J. Biomech.*, vol. 166, p. 112045, 2024.

[25] M. Jacquelin Perry, "Gait analysis: normal and pathological function," *New Jersey: SLACK*, 2010.

[26] Q. Nguyen and K. Sreenath, "Safety-critical control for dynamical

bipedal walking with precise footstep placement," *IFAC-PapersOnLine*, vol. 48, no. 27, pp. 147–154, 2015.
[27] S. M. Bruijn, O. Meijer, P. Beek, and J. H. van Dieen, "Assessing the stability of human locomotion: a review of current measures," *J. R. Soc. Interface*, vol. 10, no. 83, p. 20120999, 2013.
[28] W.-H. Chen, D. J. Ballance, P. J. Gawthrop, and J. O'Reilly, "A nonlinear disturbance observer for robotic manipulators," *IEEE Trans. Ind. Electron.*, vol. 47, no. 4, pp. 932–938, 2000.
[29] M. Yu and G. Lv, "Task-invariant centroidal momentum shaping for lower-limb exoskeletons," in *Conf. Decis. Control*. IEEE, 2022, pp. 2054–2060.
[30] R. Cham and M. S. Redfern, "Lower extremity corrective reactions to slip events," *J. Biomech.*, vol. 34, no. 11, pp. 1439–1445, 2001.
[31] S. Madgwick *et al.*, "An efficient orientation filter for inertial and inertial/magnetic sensor arrays," *Report x-io and University of Bristol (UK)*, vol. 25, pp. 113–118, 2010.
[32] H. M. Cho, I. Kang, D. Park, D. D. Molinaro, and A. J. Young, "Real-time walk detection for robotic hip exoskeleton applications," in *Proc. Int. Symp. Med. Robot.* IEEE, 2022, pp. 1–5.
[33] B. Stellato, G. Banjac, P. Goulart, A. Bemporad, and S. Boyd, "OSQP: an operator splitting solver for quadratic programs," *Math. Program. Comput.*, vol. 12, no. 4, pp. 637–672, 2020.
[34] D. A. Winter, *Biomechanics and Motor Control of Human Movement*. John Wiley & Sons, 2009.
[35] H. Debelle, C. N. Maganaris, and T. D. O'Brien, "Biomechanical mechanisms of improved balance recovery to repeated backward slips simulated by treadmill belt accelerations in young and older adults," *Front. Sports Act. Living*, vol. 3, p. 708929, 2021.
[36] E. R. Westervelt, J. W. Grizzle, C. Chevallereau, J. H. Choi, and B. Morris, *Feedback control of dynamic bipedal robot locomotion*. NW Boca Raton, FL: CRC press, 2018.
[37] I. Farkhatdinov, J. Ebert, G. Van Oort, M. Vlutters, E. Van Asseldonk, and E. Burdet, "Assisting human balance in standing with a robotic exoskeleton," *IEEE Robot. Autom. Lett.*, vol. 4, no. 2, pp. 414–421, 2019.
[38] P. R. Golyski, N. K. Swaich, F. A. Panizzolo, and G. S. Sawicki, "Effects of an elastic hip exoskeleton on stability quantified by mechanical energetics and whole-body angular momentum during walking with treadmill belt speed perturbations," *J. Biomech.*, p. 112784, 2025.
[39] D. A. Neumann, "Kinesiology of the hip: a focus on muscular actions," *J Orthop Sports Phys Ther.*, vol. 40, no. 2, pp. 82–94, 2010.
[40] Vicon, *Plug-in-Gait Modelling Instructions*, Vicon Motion Systems, Oxford, UK, 2002, vicon Manual. Oxford Metrics Ltd.
[41] A. Rajagopal, C. L. Dembia, M. S. DeMers, D. D. Delp, J. L. Hicks, and S. L. Delp, "Full-body musculoskeletal model for muscle-driven simulation of human gait," *IEEE Trans. Biomed. Eng.*, vol. 63, no. 10, pp. 2068–2079, 2016.
[42] E. Reznick, K. R. Embry, R. Neuman, E. Bolívar-Nieto, N. P. Fey, and R. D. Gregg, "Lower-limb kinematics and kinetics during continuously varying human locomotion," *Sci. Data*, vol. 8, no. 1, p. 282, 2021.
[43] D. D. Molinaro, K. L. Scherpereel, E. B. Schonhaut, G. Evangelopoulos, M. K. Shepherd, and A. J. Young, "Task-agnostic exoskeleton control via biological joint moment estimation," *Nature*, vol. 635, no. 8038, pp. 337–344, 2024.
[44] C. K. Perera, A. A. Gopalai, S. A. Ahmad, and D. Gouwanda, "Muscles affecting minimum toe clearance," *Frontiers in Public Health*, vol. 9, p. 612064, 2021.
[45] M. Afschrift, L. Pitto, W. Aerts, R. van Deursen, I. Jonkers, and F. De Groote, "Modulation of gluteus medius activity reflects the potential of the muscle to meet the mechanical demands during perturbed walking," *Sci. Rep.*, vol. 8, no. 1, p. 11675, 2018.
[46] T. Namayeshi, R. Haddara, D. Ackland, and P. V. S. Lee, "The role of the ankle plantar flexor muscles in trip recovery during walking: a computational modeling study," *Front. Sports Act. Living*, vol. 5, p. 1153229, 2023.
[47] L. H. Sloot, J. C. Van Den Noort, M. M. Van Der Krogt, S. M. Bruijn, and J. Harlaar, "Can treadmill perturbations evoke stretch reflexes in the calf muscles?" *PloS one*, vol. 10, no. 12, p. e0144815, 2015.
[48] T. D. O'Brien, N. D. P. Reeves, V. Baltzopoulos, D. A. Jones, and C. N. Maganaris, "In vivo measurements of muscle specific tension in adults and children," *Exp. Physiol.*, vol. 95, no. 1, pp. 202–210, 2010.
[49] T. Negishi and N. Ogihara, "Regulation of whole-body angular momentum during human walking," *Sci. Rep.*, vol. 13, no. 1, p. 8000, 2023.
[50] M. Van Mierlo, J. Ambrosius, M. Vlutters, E. Van Asseldonk, and H. Van Der Kooij, "Recovery from sagittal-plane whole body angular momentum perturbations during walking," *J. Biomech.*, vol. 141, p. 111169, 2022.
[51] H. Debelle, C. Harkness-Armstrong, K. Hadwin, C. N. Maganaris, and T. D. O'Brien, "Recovery from a forward falling slip: measurement of dynamic stability and strength requirements using a split-belt instrumented treadmill," *Front. Sports Act. Living*, vol. 2, p. 82, 2020.